eNeuro

Research Article: New Research | Disorders of the Nervous System

Long-Term Deficits in Cortical Circuit Function after Asphyxial Cardiac Arrest and Resuscitation in Developing Rats

Cortical circuit deficits after cardiac arrest

Jason W. Middleton[1], Daniel J. Simons[2], Jennifer W. Simmons[3], Robert S.B. Clark[4,5], Patrick M. Kochanek[4,5] and Michael Shoykhet[3]

[1]*Department of Cell Biology and Anatomy, Neuroscience Center of Excellence, Louisiana State University Health Sciences Center, New Orleans, LA 70112*

[2]*Department of Neurobiology, University of Pittsburgh School of Medicine, Pittsburgh, PA 15261*

[3]*Department of Pediatrics, Washington University in St. Louis School of Medicine, St. Louis, MO 63110*

[4]*Department of Critical Care Medicine, University of Pittsburgh School of Medicine, Pittsburgh, PA 15261*

[5]*Safar Center for Resuscitation Research, University of Pittsburgh, Pittsburgh, PA 15260*

DOI: 10.1523/ENEURO.0319-16.2017

Received: 20 October 2016

Revised: 8 June 2017

Accepted: 9 June 2017

Published: 19 June 2017

Author Contributions: JWM, DJS, RSBC, PMK and MS Designed Research. JWM, JWS and MS Performed Research and Analyzed Data. JWM, DJS, RSBC, PMK and MS Wrote the paper.

Funding: HHS | NIH | National Institute of Neurological Disorders and Stroke (NINDS): 100000065; K08 NS082362. HHS | NIH | National Institute of Neurological Disorders and Stroke (NINDS): 100000065; NS19550. HHS | NIH | Eunice Kennedy Shriver National Institute of Child Health and Human Development (NICHD): 100009633; HD045968. HHS | NIH | Eunice Kennedy Shriver National Institute of Child Health and Human Development (NICHD): 100009633; 5K12 HD04739-8. HHS | NIH | Eunice Kennedy Shriver National Institute of Child Health and Human Development (NICHD): 100009633; K12 HD 01487. Children's Discovery Institute (CDI): 100009340; FR-2011-145. WUSTL | McDonnell Center for Systems Neuroscience: 100009607.

Conflict of Interest: Authors report no conflict of interest.

This study was supported by NIH Grants K08 NS-082362 (to M.S.), NS19950 (to D.J.S.) and HD045968 (to R.S.B.C.). M.S. was also supported by the Pediatric Critical Care Scientist Development Program (5K12-HD04739-8, University of Utah), Children's Discovery Institute of the St. Louis Children's Hospital, McDonnell Center for Systems Neuroscience and Child Health Research Center of Excellence in Developmental Biology at Washington University School of Medicine (K12-HD01487).

Correspondence should be addressed to either Michael Shoykhet, MD, PhD, Division of Pediatric Critical Care Medicine, Department of Pediatrics, Washington University in St. Louis School of Medicine, Box 8208, 660 S. Euclid Avenue, St. Louis, MO 63110. e-mail: Shoykhet_m@wustl.edu or Jason W. Middleton, PhD, Department of Cell Biology and Anatomy, Neuroscience Center of Excellence, School of Medicine, Louisiana State University Health Sciences Center, New Orleans, LA 70112. E-mail: jmidd3@lsuhsc.edu

Cite as: eNeuro 2017; 10.1523/ENEURO.0319-16.2017

1. Manuscript Title

Long-term deficits in cortical circuit function after asphyxial cardiac arrest and resuscitation in developing rats

2. Abbreviated Title

Cortical circuit deficits after cardiac arrest

3. Authors

Jason W. Middleton[1], Daniel J. Simons[2], Jennifer W. Simmons[3], Robert S.B. Clark[4,5], Patrick M. Kochanek[4,5], and Michael Shoykhet[3]

Author Affiliations:

1. Department of Cell Biology and Anatomy, Neuroscience Center of Excellence, Louisiana State University Health Sciences Center, New Orleans, LA, 70112.
2. Department of Neurobiology, University of Pittsburgh School of Medicine, Pittsburgh, PA, 15261.
3. Department of Pediatrics, Washington University in St. Louis School of Medicine, St. Louis, MO, 63110
4. Department of Critical Care Medicine, University of Pittsburgh School of Medicine, Pittsburgh, PA, 15261.
5. Safar Center for Resuscitation Research, University of Pittsburgh, Pittsburgh, PA, 15260.

4. Author Contributions

JWM, DJS, RSBC, PMK and MS Designed Research. JWM, JWS and MS Performed Research and Analyzed Data. JWM, DJS, RSBC, PMK and MS Wrote the paper

5. Correspondence should be addressed to

Michael Shoykhet, MD, PhD
Division of Pediatric Critical Care Medicine
Department of Pediatrics
Washington University in St. Louis School of Medicine
Box 8208
660 S. Euclid Avenue
St. Louis, MO 63110
e-mail: Shoykhet_m@wustl.edu
and

Jason W. Middleton, PhD
Department of Cell Biology and Anatomy
Neuroscience Center of Excellence
School of Medicine
Louisiana State University Health Sciences Center
New Orleans, LA 70112
e-mail: jmidd3@lsuhsc.edu

6. Number of Figures: 9
7. Number of Tables: 1
8. Number of Multimedia: 0
9. Number of words for Abstract: 250
10. Number of words for Significance Statement: 99
11. Number of words for Introduction: 561
12. Number of words for Discussion: 1288

13. Acknowledgements

The authors thank Henry Alexander for excellent technical assistance with the cardiac arrest model.

14. Conflict of Interest

Authors report no conflict of interest.

15. Funding Sources

This study was supported by NIH Grants K08 NS-082362 (to M.S.), NS19950 (to D.J.S.) and HD045968 (to R.S.B.C.). M.S. was also supported by the Pediatric Critical Care Scientist Development Program (5K12-HD04739-8, University of Utah), Children's Discovery Institute of the St. Louis Children's Hospital, McDonnell Center for Systems Neuroscience and Child Health Research Center of Excellence in Developmental Biology at Washington University School of Medicine (K12-HD01487).

Abstract

Cardiac arrest is a common cause of global hypoxic-ischemic brain injury. Poor neurologic outcome among cardiac arrest survivors results not only from direct cellular injury but also from subsequent long-term dysfunction of neuronal circuits. Here, we investigated the long-term impact of cardiac arrest during development on the function of cortical Layer IV (L4) barrel circuits in the rat primary somatosensory cortex. We used multi-electrode single neuron recordings to examine responses of presumed excitatory L4 barrel neurons to controlled whisker stimuli in adult (8 ± 2 mo old) rats that had undergone 9 min of asphyxial cardiac arrest and resuscitation during the 3rd postnatal week. Results indicate that responses to topographically appropriate "principal" whisker (PW) deflections are smaller in magnitude in cardiac arrest survivors than in control rats. Responses to adjacent whisker (AW) deflections are similar in magnitude between the two groups. Due to a disproportionate decrease in PW-evoked responses, receptive fields of L4 barrel neurons are less spatially focused in cardiac arrest survivors than in control rats. In addition, spiking activity among L4 barrel neurons is more correlated in cardiac arrest survivors than in controls. Computational modeling demonstrates that experimentally-observed disruptions in barrel circuit function after cardiac arrest can emerge from a balanced increase in background excitatory and inhibitory conductances in L4 neurons. Experimental and modeling data together suggest that after a hypoxic-ischemic insult, cortical sensory circuits are less responsive and less spatially tuned.

Modulation of these deficits may represent a therapeutic approach to improving neurologic outcome after cardiac arrest.

Significance Statement

Cardiac arrest survivors often suffer severe neurologic injury. Neurologic injury and subsequent behavioral deficits likely arise not only from arrest-related cell death but also from long-term dysfunction of neuronal circuits. We show in a rat model of pediatric asphyxial cardiac arrest that deficits in sensory information processing persist in cortical Layer IV circuits for months after injury. As a general feature, hypoxic-ischemic brain injury leads to less responsive and less spatially tuned sensory cortical circuits. Understanding mechanisms underlying abnormal circuit function after cardiac arrest may lead to new approaches for modulating neuronal circuits and restoring normal function in survivors.

Introduction

Cardiac arrest (CA) occurs when all blood flow to the body, including to the brain, ceases. Annually in the US, CA affects ~350,000 adults (CDC, 2002; Roger et al., 2012) and ~10,000 children (Atkins et al., 2009). In adults, CA occurs most commonly as a result of cardiac ischemia and subsequent arrhythmia. In children, CA often follows respiratory compromise and resulting hypoxia/asphyxia. Regardless of the etiology, survival after CA critically depends on timely initiation of cardiopulmonary resuscitation (CPR) (Valenzuela et al., 1997; Karch et al., 1998; Gottschalk et al., 2002; De Maio et al., 2003; Weisfeldt et al., 2011). Rescuers in well-developed Emergency Response Systems (ERS) arrive and initiate CPR 6-8 minutes after ERS activation (Bernard et al., 2002; The Hypothermia after Cardiac Arrest Study Group, 2002; Bernard et al., 2010; Deasy et al., 2010; Aufderheide et al., 2011; Zive et al., 2011; Wang et al., 2012). Despite such short response times, <10% of CA victims recover good neurologic function (Graves et al., 1997; Aufderheide et al., 2011; Mateen et al., 2011). Even in witnessed in-hospital pediatric CA with immediate onset of CPR and return of spontaneous circulation within 15 minutes, only 30% of victims survive with a good neurologic outcome (Matos et al., 2013). Thus, timely CPR restores blood flow, but resulting global hypoxic-ischemic brain injury often precludes meaningful neurologic recovery.

Neuronal cell death after 10-15 minutes of CA cannot fully explain the extent of neurologic injury observed in survivors. In animal CA models, 9-10 minutes of arrest results only in modest neuronal cell death (Myers and

Yamaguchi, 1977; Pulsinelli and Brierley, 1979; Kumar et al., 1988; Radovsky et al., 1997; Bottiger et al., 1998; Geocadin et al., 2000; Shoykhet et al., 2012). Nine minutes of asphyxial CA in developing rats leads to persistent dysfunction among whisker-responsive thalamocortical (TC) neurons in the Ventroposterior medial nucleus (VPm) without overt cell death in VPm or among reciprocally-connected inhibitory neurons in the Reticular Nucleus (RT) (Shoykhet et al., 2012). Similarly, in neonatal animals, a moderate hypoxic-ischemic insult impairs monocular deprivation-induced circuit reorganization in the visual cortex without overt loss of inhibitory neurons (Failor et al., 2010). A ten minute-long CA produces wide-spread ultrastructural alterations in ribosomes, mitochondria and endoplasmic reticulum among neurons in the hippocampus, RT and cerebral cortex despite only a 20% cell loss in the hippocampus (Hossmann et al., 2001) and paucity of cell death in the thalamus and cortex (Radovsky et al., 1997). Finally, rats resuscitated from a 5 minute-long CA demonstrate sustained neurobehavioral deficits (Schreckinger et al., 2007) even though such short arrests produce minimal cell death (Radovsky et al., 1995). Why do neurologic deficits persist even when neuronal cell death is modest? We propose that long-term neuronal circuit dysfunction after injury contributes to sustained neurologic deficits in CA survivors.

Here, we characterize long-term abnormalities of cortical Layer IV (L4) 'barrel' circuits in adult rats that survived an asphyxial CA during development. Layer IV is the major thalamorecipient zone in the somatosensory cortex. Because other cortical layers depend on information propagated from L4, CA-

associated abnormalities in L4 can have widespread adverse consequences. In this clinically-realistic model, neuronal death in the cerebral cortex is observed only in a subset of L5 neurons (Fink et al., 2004; Shoykhet et al., 2012). Yet, we find circuit-level abnormalities in L4 that persist for >6 months after arrest, suggesting long-term circuit reorganization in survivors.

Methods

Animals

Thirteen Sprague-Dawley female rats were used in the experiments. CA or sham intervention was carried out at post-natal day (PND) 16-18, and neurophysiologic recordings were carried out on adult rats at least 6 months after arrest. Only female rats were used in the study because the large weight (>600 g) of adult male rats in captivity presents a number of logistical and technical difficulties. First, rats this large require single housing, which is not recommended by IACUC and Federal regulations. Second, surgical procedures in preparation for recordings (tracheostomy, arterial and venous line placements, craniotomy) become more complex due to large amounts of fat overlying surgical landmarks and result in higher surgical mortality due to excessive bleeding associated with fat dissection. Third, overweight male rats require high inflation pressures (>25-30 cm H_2O) to maintain adequate ventilation and oxygenation during the recordings, which leads to ongoing barotrauma, results in rapid physiologic deterioration, and limits recording time. Finally, male rats under fentanyl analgesia used during the recordings fail to urinate spontaneously due to

sphincter constriction. Progressive bladder distention, if not addressed surgically with a suprapubic catheter, evokes abnormal autonomic responses and further impairs pulmonary dynamics, substantially degrading recording validity and quality. For these reasons, we focused our study on female rats. Although pediatric CA occurs more commonly in males (~65% male vs. 35% female) (Moler et al., 2015), hypoxic-ischemic brain injury tends to be less severe in females (for review, see (Johnston and Hagberg, 2007). Hence, the abnormalities observed in female rats in the current study may be milder than those in male rats. Animals were housed in AALAC-certified facility on a 12 hr light-dark cycle with free access to food and water. The [Author University] Animal Care and Use Committee approved all experimental procedures.

Asphyxial cardiac arrest

Female PND16-18 Sprague-Dawley rats (35–40g) were anesthetized with 3% isoflurane/50% N_2O/balance oxygen, endotracheally intubated with an 18-gauge angiocatheter and mechanically ventilated with 1-2% isoflurane/50% N_2O/balance oxygen for surgery (Harvard Apparatus, Cambridge, MA). Femoral arterial and venous catheters were placed through skin incisions under sterile condition, and needle electrocardiogram (EKG) electrodes and needle scalp electroencephalogram (EEG) electrodes were inserted. Mean arterial blood pressure, EKG, and EEG were continuously monitored and recorded (Model 7 Polygraph, Grass Instruments, West Warwick, RI). Minute ventilation was titrated to maintain normal arterial pCO_2 (~40±2 mmHg). Vecuronium (1 $mg \cdot kg^{-1}$,

intravenously; Sun Pharmaceutical, Gujarat, Ind) was administered 10 minutes before asphyxia to establish neuromuscular blockade. Vecuronium was chosen for its short (15-20 min) duration of action in rats, such that subsequent recovery is not affected by the neuromuscular blockade. Two minutes prior to arrest, the anesthetic gas mixture was turned off, and the rat was ventilated with room air (FiO_2 = 0.21). This anesthetic washout was performed to reduce the confounding effects of inhaled anesthetics (Weigl et al., 2005; Statler et al., 2006; Bickler et al., 2012).

Previous pilot experiments demonstrated that electroencephalographic activity begins to recover in frequency and amplitude 2 minutes after discontinuation of the anesthetic mixture. At this time, the animals are beginning to emerge from general anesthesia but have yet to regain consciousness. Therefore, at the end of the 2 minute-long washout period, the ventilator was turned off for 9 minutes. With this experimental paradigm, apnea inevitably leads to pulseless CA within 60-90 seconds as demonstrated by the arterial waveform. At the end of the 9 minute period of asphyxia, the rats were resuscitated using a clinically-realistic algorithm based on the guidelines for human Advanced Cardiac Life Support (AHA, 2006). Mechanical ventilation was restarted with 100% O_2 (FiO_2 = 1.0), intravenous epinephrine (0.005 mg/kg) and sodium bicarbonate (1 mEq/kg) were administered, and manual chest compressions (approx. 300/minute) were performed until either return of spontaneous circulation (ROSC) or 2 minutes had elapsed from initiation of resuscitation. If rats did not attain ROSC within 2 minutes of resuscitation, they were euthanatized.

After resuscitation, vascular catheters were removed, all surgical incisions were closed, and rats were weaned from mechanical ventilation. Rats that failed to separate from mechanical ventilation by 1 hour after CA were euthanatized. After extubation, rats were observed in FiO_2 = 1.0 for 1 hr to mimic a clinical scenario and then returned to their mothers. Pups were kept with their mother until PND28 and then weaned. Shams underwent all procedures except asphyxia and resuscitation. Survival rate in this model of cardiac arrest is ~85% (Fink et al., 2004), with mortality mostly occurring within the first 24-48 hours due to the animal's poor neurologic condition. Ten rats underwent cardiac arrest, 2 were euthanatized within 48 hours post-arrest due to inability to self-care, and 8 survived long-term to undergo recordings. Mortality in the sham group is rare, such that all 5 rats that underwent a sham surgery survived to undergo recordings. The age of the rats at the time of recordings was 8±2 months.

Surgical preparation for neurophysiologic recordings

Rats were anesthetized with isoflurane, and a tracheal tube was inserted via tracheostomy to maintain a clear air passage. Tracheostomy is required to allow unimpeded access to the whiskers for stimulation and to allow for suctioning of secretions from the airway during the recording session. Small diameter silastic tubing was inserted into the external jugular vein for drug delivery, and a small Teflon catheter was inserted into the right femoral artery for monitoring blood pressure. The skull was exposed, and small stainless steel screws were inserted into the bone over the left occipital and frontal lobes for electrocorticogram

(ECoG) monitoring; an additional screw was inserted into the bone over the right frontal lobe to serve as a reference for cortical microelectrode recordings. Bone overlying the right primary somatosensory cortex was thinned with a handheld microdrill. For unit recordings, a small area (< 0.5 x 0.5 mm^2) of thinned bone was removed overlying the right barrel cortex (~3 mm posterior to bregma and ~5 mm lateral to midline). Saline was periodically applied to an acrylic dam constructed around the craniotomy. All wound edges were infiltrated with 2% lidocaine at the completion of the surgical procedures.

During the recording session isoflurane was discontinued, and the rat was maintained in a lightly sedated state using fentanyl (Baxter Healthcare Corp., Deerfield, IL, 10 μg kg^{-1} h^{-1}). The rat was immobilized with pancuronium bromide (SICOR Pharmaceuticals Inc., Irvine, CA, 1.6 mg kg^{-1} h^{-1}) to prevent spontaneous whisker movements that could otherwise interfere with use of our whisker stimulators (below). We used pancuronium during the recordings due to its long duration of action. Body temperature was maintained at 37°C using a servo-controlled heating blanket (Harvard Apparatus, Hollister, MA). Blood pressure, heart rate, tracheal airway pressure, and ECoG were monitored throughout the recording session with a personal computer using custom-written software. We decided *a priori* that if we could not maintain these indicators within normal physiological ranges (mean arterial pressure > 60 mmHg, heart rate > 300, peak airway pressure < 30 cm H_2O, no seizure activity and minimal bursting on the ECoG), we would terminate the recording session. No recordings were terminated prematurely in this study.

289 Whisker stimulation

290 Whiskers were deflected one at a time using a piezoelectric stimulator attached
291 10 mm from the base of the whisker (Simons, 1983). Stimulus waveforms, stored
292 on disk, were output at 10 kHz via an eight-channel digital-to-analog converter.
293 Whiskers were randomly deflected 1 mm in one of 8 directions (0°, 45°, 90°, etc.)
294 using a "ramp-and-hold" stimulus. The ramp phase of the deflection was ~8 ms
295 long, with a mean velocity of 125 mm/s. The whisker deflection was maintained
296 for 200 ms, and the whisker was then returned to its resting or neutral position
297 with the same speed as the initial deflection.

298

299 Recording

300 Simultaneous multiple, single-unit recordings were obtained using a multi-channel
301 Eckhorn matrix (MM-5, Thomas Recording, Geissen, Germany). Platinum/iridium
302 in quartz fibers (60 µm diameter) were pulled and ground to 2-5 µm tip
303 diameters, having impedances of 1-6 MΩ. One-by-one, electrodes were brought
304 into contact with the pial surface and advanced into Layer IV (~700 µm below the
305 pial surface) before positioning of the next electrode. The Eckhorn matrix and the
306 accompanying software allow for independent movement of each electrode in the
307 z-axis. Typically, 3 electrodes inserted into the brain 100-200 µm apart were used
308 simultaneously in each recording session. After characterizing a single neuron on
309 a given electrode, that electrode was advanced in 4 steps until a spike from a
310 different neuron was encountered. Usually, an electrode is moved 50-100 µm
311 from the prior recording depth to optimize waveform discrimination of the newly

312 encountered neuron. After traversing a full depth of Layer IV (700-1000 μm
313 below the pial surface) the electrode was withdrawn from the brain and
314 repositioned 20-50 μm away from the previous recording location without
315 disturbing the other electrodes in the array.

316 The principal whisker (PW) of a cortical neuron is defined as the whisker
317 whose deflection evokes the largest spiking response relative to other whiskers
318 (Fig. 1). The adjacent whiskers (AWs) were defined as whiskers immediately
319 rostral, caudal, dorsal and ventral to the PW (Fig. 1B). The PW corresponds
320 anatomically to the barrel in which the recorded neuron is located (Fig. 1C). This
321 relationship was later confirmed by histological analysis. Microelectrode signals
322 were bandpass filtered (300 Hz – 10 kHz) and passed to a personal computer
323 where spike waveforms were detected in real time using custom-programmed
324 acquisition software (Labview, National Instruments, Austin, TX) and stored for
325 further analysis. Unless otherwise reported, means and standard errors are the
326 population means of 34 neurons recorded in 5 Sham rats and 57 neurons
327 recorded in 8 CA rats.

328

329 Data analysis

330 Action potential firing, or spiking, evoked by whisker deflections was
331 characterized by magnitude of responses and stimulus-specificity. For each
332 neuron, response magnitudes to deflection onsets (ON) and offsets (OFF) were
333 quantified as the average number of spikes per stimulus discharged in the
334 appropriate 25 ms long response window (Fig 1D). Receptive fields (RFs) are

defined as the set of whiskers which evoke a spiking response in individual L4 neurons (Simons and Carvell, 1989). For each cell, RF focus was quantified by calculating the ratio of responses to adjacent and principal whiskers (AW/PW ratio). Small or large AW/PW ratios indicate narrow or broad spatial focus on the PW respectively. An average AW value was calculated for each neuron by using the responses to different AWs for that particular neuron. Depending on the recording and whisker stimulation conditions, between 1 and 4 AWs contributed to this average for each neuron.

Putative excitatory cells generate regular spike (RS) extracellular waveforms characterized by an asymmetric biphasic waveform with a broad initial negative component (200-400 μs; Fig. 1E) (Bruno and Simons, 2002). Putative inhibitory cells generate fast spike (FS) extracellular waveforms, which are characterized by a more symmetric biphasic waveform with a fast initial negative component (100-180 μs) (Bruno and Simons, 2002). This study focused specifically on RS cells for two reasons. First, FS neurons constitute ~10% of L4 barrel neurons (Beaulieu, 1993), and hence occur less frequently in extracellular recordings. For example, in this study we recorded 4 and 8 FS neurons in sham and CA rats, respectively (~1 FS neuron/rat), which is insufficient for quantitative comparisons. Second, unambiguous identification of FS neurons in extracellular recordings requires special processing of electrodes and specific filter settings, which makes simultaneous recording of FS and RS neurons challenging (Bruno and Simons, 2002). Spike waveforms were examined with cluster analysis using custom programmed software in Labview. Recorded spike waveforms were

sorted into unit clusters off-line using principal component analysis in 2D space. Cut clusters were then examined to remove outlier (non-similar) waveforms. Interspike interval (ISI) histograms were checked for each unit to ensure absence of ISIs < 1 ms, which corresponds to the absolute refractory period. Only well-isolated units with uniform action potential waveforms and interspike intervals that respect the absolute refractory period were used in the analyses (Fig. 1E-G). After sorting, mean spike waveforms were calculated and the duration of early and late components of the waveforms were measured. A two dimensional scatterplot of these two components reveals two clusters (Bruno and Simons, 2002), and cell type identity was assigned based on this criteria. Individual, well-isolated units were recorded on different electrodes of the multi-electrode array. Only one unit was taken from a single microelectrode.

Correlation of spiking activity between pairs of simultaneously recorded cells was quantified by the joint post stimulus histogram (jPSTH). The jPSTH is a 2-dimensional plot that gives the number of coincident spikes as a function of the relative spike times of the 2 compared neurons:

$$\mathrm{jPSTH}(t_i, t_j) = \sum_k \delta_1^k(t_i)\delta_2^k(t_j) \qquad (1)$$

where δ_n^k is the k^{th} trial of the spike train of neuron 1 or 2. To quantify the number of coincidences above chance level we subtract a trial-shuffled version of the jPSTH from the trial-matched version, giving the shuffle-corrected jPSTH. The correlation is computed by taking the diagonal of the shuffle corrected jPSTH and dividing it by the product of the individual PSTHs:

$$\text{correlation}(t) = \frac{\text{jPSTH}(t,t)}{PSTH_1(t)PSTH_2(t)} \qquad (2)$$

All data analyses were performed on whisker responses from 80 trials – 10 repetitions of each of the 8 angular directions. Spike counts, PSTHs and jPSTHs were averaged over 80 trials before being used to calculate population means.

Histology

Upon termination of an experiment, the rat was deeply anesthetized with sodium pentobarbital (100 mg/kg, iv) and transcardially perfused (2% paraformaldehyde and 1.5% glutaraldehyde in 0.1 M phosphate buffer) for cytochrome oxidase (CO) histochemistry (Wong-Riley et al., 1978). The cortex was cut tangentially (60 µm sections), and sections were reacted for CO and counterstained with thionin. Using microdrive readings, signs of tissue disruption, and electrolytic lesions made during the experiment, recording sites were localized with respect to individual underlying barrels. Histological evaluation indicated that there was no systematic difference between sham and CA rats with respect to recording locations. In an independent cohort of CA (n=5) and sham rats (n=5), used for recordings elsewhere in the brain and subjected to an identical experimental paradigm, the brains were cut in a coronal plane and stained with thionin. In this cohort, cortical thickness was measured in the motor cortex and in the whisker subfield of the primary somatosensory (barrel) cortex between 2.6 to 3.0 mm posterior to bregma (Paxinos and Watson, 2007). Measurements were not corrected for shrinkage. However, all brains were processed similarly with expected shrinkage of ~30%. Image manipulation was limited to auto-contrast,

auto-tone and auto-color adjustments in Adobe Photoshop and was applied to the entire image.

Computational Modeling and Simulations

A leaky integrate-and-fire neuron model was used to simulate the voltage dynamics and spiking activity of layer 4 neurons (Gabbiani and Cox, 2010). The model has the form:

$$C\frac{dV}{dt} = -g_{leak}\cdot(V - V_{leak}) + \mu + I_{background} + I_{whisk} \qquad (3)$$

where C is the membrane capacitance, g_{leak} and V_{leak} are the conductance and reversal potential for the leak current, μ is the bias current and $I_{background}$ and I_{whisk} are the currents from background and whisker-driven synaptic sources, respectively. The background currents represent synaptic inputs from non-stimulus driven sources, and thus on-going, spontaneous background fluctuating input currents. The background current follows the form:

$$I_{background} = -\sigma_E g_E(t)\cdot(V - V_E) - \sigma_I g_I(t)\cdot(V - V_I) \qquad (4)$$

where σ is the maximal conductance scaling factor and V is the reversal potential for the background synaptic currents; the subscripts E and I refer to excitatory and inhibitory components, respectively. The time dependent conductance, $g(t)$, is described by the following:

$$g(t) = \sum_i a(t_i) \qquad (5)$$

The function, $a(t)$, is the timecourse of a unitary synaptic event at time t_i according to:

$$a(t) = \alpha^2 t \cdot e^{-\alpha t} \qquad (6)$$

The rates of unitary excitatory and inhibitory synaptic conductances are $r_{E,\ background}$ and $r_{I,\ background}$, respectively. The timescale of synaptic conductances generated in this manner is given by: $\tau = 1/\alpha$. The occurrence times of background excitatory and inhibitory synaptic events are Poisson distributed.

Similarly, the current evoked in a model L4 neuron by whisker deflection is given as a combination of thalamocortical-driven monosynaptic excitatory and TC-driven disynaptic inhibitory currents:

$$I_{whisk} = -\sigma_{E,whisk} g_{E,whisk}(t) \cdot (V - V_E) - \sigma_{I,whisk} g_{I,whisk}(t) \cdot (V - V_I) \qquad (7)$$

where the time-dependent conductances, *g(t)*, have the same functional form as the background components.

The rate of whisker-driven **cortical** excitatory and inhibitory currents is given by:

$$r_{whisk}(t) = \begin{cases} r_{spont}, & t < twhisk \\ r_{spont} + \dfrac{\beta_{evoked}\left(e^{-\frac{t-t_{whisk}}{\tau_2}} - e^{-\frac{t-t_{whisk}}{\tau_1}}\right)}{\tau_2 - \tau_1}, & t \geq twhisk \end{cases} \qquad (8)$$

where r_{spont} is the spontaneous firing rate, τ_1 and τ_2 are the time constants for the rise and fall of the time-dependent firing rate and β_{evoked} is the firing rate scaling factor. The unitary synaptic conductance times are Poisson distributed according to this time-varying rate.

To study output spike correlations between a pair of neurons, we defined an additional parameter, *c*, which controlled the correlation of the two input

440 synaptic conductances. To each input conductance, independent events were
441 added with a rate of *r(1-c)* and common events with a rate of *rc*.

442 The chosen spike threshold values are within the range observed in the
443 cortex (Dembrow et al., 2010; Pidoux et al., 2011). Maximal values for synaptic
444 conductances are consistent with those used in other cortical network models
445 (Lisman et al., 1998). These conductance values result in synaptic potentials with
446 amplitudes <1 mV, consistent with experimentally observed amplitudes for
447 thalamocortical (Bruno and Sakmann, 2006) and intracortical (Lefort et al., 2009)
448 synaptic potentials. Timescales for the stimulus-evoked TC-driven monosynaptic
449 excitation and disynaptic inhibition were set to qualitatively reproduce the relative
450 time-varying nature of the thalamocortical excitatory and of the intracortical
451 inhibitory PSTH's (Khatri et al., 2004). The spontaneous rate of thalamocortical
452 inputs to model L4 cortical neurons is based on experimentally observed
453 spontaneous firing rate of VPm neurons (Simons and Carvell, 1989; Shoykhet
454 and Simons, 2008) combined with the estimated level of thalamocortical
455 convergence onto L4 regular spike units (RSUs) (Bruno and Sakmann, 2006).
456 The timescales of the synaptic conductances are within the range observed at
457 thalamocortical (Higley and Contreras, 2006) and intracortical synapses (Oswald
458 and Reyes, 2008, 2011).

459 The parameters of the model, unless otherwise specified, are as follows:
460 A) Intrinsic parameters: C = 1 mF/cm^2, g_{leak} = 0.0375 mS/cm^2, V_{leak} = -80 mV, μ =
461 32 mA/cm^2, v_{thresh} = -40.4 mV, v_{reset} = -80 mV; B) Synaptic parameters: σ_E = 0.22
462 mS/cm^2·s, $\tau_{E,\ background}$ = 5 ms, V_E = 0 mV, σ_I = 0.20 mS/cm^2·s, $\tau_{I,\ background}$ = 20

ms, V_I = -80 mV, $\sigma_{E,\ whisk}$ = 0.1 mS/cm^2·s, $\tau_{E,\ whisk}$ = 2 ms, τ_{1E} = 0.1 ms, τ_{2E} = 4 ms, $\sigma_{I,\ whisk}$ = 0.07 mS/cm^2·s, $\tau_{I,\ whisk}$ = 4 ms, τ_{1I} = 0.6 ms, τ_{2I} = 8 ms, $r_{spont,\ E}$ = 2 x 10^3/s, $r_{spont,\ I}$ = 2.3 x 10^3/s, $\beta_{evoked,\ E}$ = 4 x 10^3, $\beta_{evoked,\ I}$ = 4.2 x 10^3.

Statistics

All statistical analyses were performed in Matlab. Data are presented as mean ± SEM. Sample size is the number of RSUs recorded in each experimental group. Recordings and analyses were performed by an experimenter blinded to injury status. *In vivo* recording data were analyzed as shown in Table 1.

Table 1. Statistical Analyses

Compared Values	Data Structure	Type of Test	p Value	Cohen's d'
AW/PW Ratio	Not normal	Wilcoxon Rank Sum	<0.001	0.73
PW ON response	Not normal	Wilcoxon Rank Sum	<0.002	0.87
AW ON response	Not normal	Wilcoxon Rank Sum	0.6846	0.12
Spontaneous firing rate	Not normal	Wilcoxon Rank Sum	0.08	0.27
Motor Cortex Thickness	Normal	Student's *t*-test	0.67	0.29
Barrel Cortex Thickness	Normal	Student's *t*-test	0.80	0.33

Results

We recorded responses of L4 barrel cortex neurons to whisker deflections in sham rats and in rats subjected early in life to a 9 minute-long CA followed by resuscitation. Single-neuron recordings of RSUs (Fig. 1E-G), which correspond

479 to excitatory neurons (Simons, 1978; Bruno and Simons, 2002), located within
480 barrel centers in L4 are included in the analyses. We analyzed data from 34
481 RSUs in 5 sham animals and from 57 RSUs in 8 CA rats.
482
483 RSU receptive fields are less spatially focused in CA survivors
484 The rat whisker pad is comprised of an ordered array of whiskers that are
485 identified by the row (lettered) and column (numbered) they occupy (Fig. 1A). L4
486 neurons in primary somatosensory cortex respond robustly to whisker deflection
487 onsets and offsets (Simons, 1978). The whisker that evokes the most robust
488 response, called the principal whisker (PW), corresponds anatomically to the
489 barrel in which that neuron is recorded (Fig. 1A-D). The whiskers immediately
490 adjacent to the PW (AWs, shown schematically in Fig. 1B and represented as
491 whiskers C3, D2, D4 and E3 surrounding the D3 PW in panel 1A) normally evoke
492 no or much smaller response (Simons and Carvell, 1989). Figure 1C shows a
493 tangential section of the L4 barrel field where the recording location of an RSU
494 with a PW functionally identified as the D3 whisker is confirmed by an electrolytic
495 lesion in the anatomically corresponding D3 barrel
496 For a normal L4 RSU, spontaneous and PW-evoked firing is sparse on a
497 single trial basis but the trial-averaged PSTH is nevertheless robustly temporally
498 locked to whisker deflection (Fig. 1H). Example sets of responses of L4 neurons
499 from sham (Fig.1I) and CA (Fig. 1J) rats illustrate typical differences in receptive
500 field (RF) structure arising from CA-induced hypoxia-ischemia. In sham rats, like
501 in normal rats (Simons and Carvell, 1989; Shoykhet et al., 2005; Shoykhet and

Simons, 2008), the PW response is much larger than the AW response (Fig. 1I). In contrast, in CA rats the PW response is similar in magnitude to the AW response (Fig. 1J).

To quantify the stimulus-specificity of receptive fields among Layer 4 neurons in sham and in CA rats, we calculated a measure of RF focus as the ratio of the AW-evoked response to the PW-evoked response for each neuron (i.e. AW/PW response ratio). A smaller AW/PW ratio indicates a more narrowly focused RF, i.e. an RF more spatially-focused on the PW. Conversely, a larger AW/PW ratio indicates a more broadly focused RF, i.e. an RF less spatially-focused on the PW. Hence, we compared the AW/PW ratios of L4 RSUs between CA and sham rats. The mean AW/PW ratio of RS neurons in CA rats is increased two-fold compared to that in sham rats (0.49 ± 0.03 vs. 0.23 ± 0.03; Wilcoxon rank sum test (WRST), $p < 0.001$; Fig. 2A). This finding suggests that RS neurons have broader, less PW-specific receptive fields several months after CA.

The difference in AW/PW ratios can arise from differences in PW responses, from differences in AW responses or from a combination of both. We found that PW-evoked responses of RS neurons are reduced by 44% in CA rats compared to sham rats (CA: 0.50 ± 0.04 spikes; sham: 0.89 ± 0.11 spikes, respectively; WRST, $p < 0.002$; Fig. 2b). In contrast, AW-evoked responses of RS neurons are similar in CA and in sham rats (CA: 0.21 ± 0.02; sham: 0.18 ± 0.03; WRST, $p = 0.6846$; Fig. 2c). Spontaneous firing rates of L4 RSU's, calculated using the observed spike counts in the 150 ms recorded period

preceding whisker stimulation, are also similar in CA and sham rats (CA: 1.6 ± 0.4 Hz; sham: 2.5 ± 0.7 Hz; WRST, $p = 0.08$). Together, these findings indicate that RSU receptive fields in CA rats broaden due to a decrease in PW-evoked responses rather than an increase in AW-evoked responses.

Barrel Cortex Architecture is Preserved in CA Survivors

The whisker-responsive region of rodent somatosensory cortex consists in L4 of cytoarchitecturally distinct regions (barrels) that can be visualized with cytochrome oxidase immunohistochemistry (Land and Simons, 1985). Barrels form during early postnatal development and are structurally stable by PND 5 with further refinement of thalamocortical projections through PND 12 (Inan and Crair, 2007). Barrel structure can be disrupted by physical injury to whisker follicle innervation before PND 5 (Van der Loos and Woolsey, 1973) and by perinatal hypoxia-ischemia at PND 3 (Quairiaux et al., 2010). In contrast, neonatal sensory deprivation without injury to peripheral receptors preserves barrel morphology (Akhtar and Land, 1991; Land et al., 1995). Our injury model induces CA relatively late in barrel *morphological* development (PND 17-19), and we hypothesized that barrel fields would be grossly anatomically normal in CA rats. Indeed, there were no observable differences between sham and CA rats in the gross anatomical appearance of individual barrels or in the anatomical organization of the whisker barrel field (Fig. 3A and B). Barrels in CA rats had well-defined cytochrome oxidase-rich centers surrounded by Nissl-rich sides and were qualitatively similar in size to those in sham rats. In a separate cohort of

548 adult CA and sham rats used for neurophysiologic recordings elsewhere in the
549 brain, we cut the brains in a coronal plane. In CA rats, cortical laminar
550 architecture appears preserved without evidence for laminar necrosis, despite
551 clear neuronal loss (and occasional finding of coagulative necrosis) in the
552 hippocampal CA1 region (Fig. 3C-F). Cortical thickness did not differ between CA
553 and sham rats in the motor (sham = 1.55±0.10 mm, CA = 1.58±0.09 mm;
554 Student's t-test p = 0.67) or in the primary somatosensory cortex (sham =
555 1.47±0.04 mm, CA = 1.45±0.09 mm, p = 0.8).
556
557 Numerical models of sham and CA L4 neurons receiving feed-forward
558 thalamocortical inputs
559 In CA survivors, broader RSU receptive fields result from smaller PW-evoked
560 responses, even though overall neuronal excitability, as measured by
561 spontaneous firing, is unchanged. One plausible mechanism is a total increase
562 in background conductance, affecting both excitatory and inhibitory inputs. We
563 used a leaky integrate-and-fire model (see Methods) to test the hypothesis the
564 increase in conductance leads to less robust responses to PW- vs. AW-evoked
565 deflections with little or no change in overall cellular excitability. Although multiple
566 physiologic mechanisms may lead to an effective increase in conductance at the
567 soma (see Discussion), for computational simplicity we increased the
568 background conductance in the model by adjusting only the rates of balanced
569 (excitatory and inhibitory) background synaptic inputs. In the CA model,
570 background synaptic input rates were ten-fold higher than those in the sham

model. While such a rate increase is clearly not physiologic, the overall increase in conductance may reflect a combination of multiple physiologic factors, e.g. synaptic rates, peak synaptic currents and spine remodeling (see Discussion). Both excitatory and inhibitory background rates were increased by the same factor, which maintains a relative balance of opposing synaptic forces while increasing conductance variability. Reflecting the unchanged excitatory-inhibitory balance and consistent with experimental data, spontaneous firing rates in the CA and sham models remain similar (see Figs. 4 and 5 below).

In the CA model, increased background conductance decreases the mean depolarization evoked by incoming synaptic inputs. When spike thresholds are removed, the slope of mean depolarization as a function of synaptic input rate is shallower in the CA model than in the sham model (Fig. 4a). Similarly, voltage change in response to a single incoming synaptic input is smaller in the CA than in the sham model (Fig 4b). The ability of a neuron to sum synaptic currents is determined by its input resistance, which, in turn, is inversely proportional to net conductance (Softky and Koch, 1993). In the CA model, increased conductance decreases input resistance. Decreased input resistance diminishes ability of CA neurons to integrate incoming synaptic inputs above action potential threshold. A similar reduction in stimulus-evoked potentials was observed by measuring field potentials in a model of neonatal hypoxic ischemia (Quairiaux et al., 2010).

When spike thresholds are re-introduced into the models, the CA model reproduces preserved AW-evoked and reduced PW-evoked firing rates observed *in vivo*. The spiking models were tested at different thalamocortically derived

synaptic input rates, resulting in output rates that are comparable to spontaneous, AW-evoked, and PW-evoked firing rates. At synaptic input rates simulating spontaneous firing, both CA and sham models generate APs at comparable frequency (Fig. 4c, top row). Similarly, at synaptic input rates simulating AW-evoked firing, CA and sham models generate similar output firing rates (Fig. 4c, middle). However, at higher input rates mimicking PW stimulation, the CA model generates APs at a lower frequency than the sham model (Fig. 4c, bottom row).

To understand how AP threshold and subthreshold synaptic mechanisms interact to give differential responses to whisker stimuli, we examined the input-output transfer function (Fig. 5). The F-I curve (i.e. firing rate vs. input curve) quantifies the level of output as a function of input amplitude. An F-I curve with a larger slope (higher gain) reflects a neuron whose output firing rate is more sensitive to incremental increases in the amplitude of synaptic inputs. Background synaptic conductance (i.e., stimulus input-independent conductance) fluctuations can affect the output-firing rate by modulating the magnitude of voltage fluctuations and by modulating the mean membrane voltage timescale. Through the action of both of these mechanisms, the changes in the background synaptic conductance state can modulate the gain of firing rate transfer functions (Chance et al., 2002; Mitchell and Silver, 2003). Different transfer functions, effectively modulated by background activity, differentially affect spike output to whisker-evoked stimuli in sham and CA conditions.

The gain of the CA model is lower than that of the sham model, leading to decreased responses to larger input stimuli (Fig. 5). The time course of the simulated thalamocortical inputs is shown along the bottom of the F-I curve. The timescales of both AW and PW thalamocortical inputs were set to the same value, and the ratio of their amplitudes (area under the TC input curves, bottom of Fig. 5) was set to 0.4 based on previous observations (Shoykhet and Simons, 2008). Spontaneous and AW-evoked input rates lead to output rates that are comparable in both the CA and sham models. PW stimulation leads to a lower output-firing rate in the CA model due to reduced gain resulting from increased balanced (excitation and inhibition) background synaptic conductance. When we simulate the time-dependent model (Eqs. 3-7), both the sham and the CA models produce PW and AW responses (Fig. 6b) qualitatively similar to those seen in the data (Fig. 6a). Quantitatively, the sham model produces an AW/PW ratio of 0.24 whereas the CA model produces an AW/PW ratio of 0.46. These simulated results reproduce the difference between AW/PW ratios observed in L4 RSUs in sham (0.23 ± 0.03) vs CA (0.49 ± 0.03) rats *in vivo*.

We set the parameters of our models based in responses to stimulus onsets (ON). To test our model further, we examined how well the models simulate responses to stimulus offsets (OFF), a stimulus that evokes responses different from stimulus onsets in sham and CA neurons. Normally in L4 barrel RSU's, OFF responses are smaller than ON responses, but the difference is not as great as that between AW and PW responses (Simons and Carvell, 1989). Furthermore, OFF/ON ratios in barrel RSU's are smaller than those in VPm

neurons, reflecting the effects of local circuitry (Simons and Carvell, 1989; Shoykhet et al., 2012). Experimentally observed OFF/ON ratios of L4 RSU's in sham rats (0.71±0.06) are comparable to those of L4 RSU's in CA rats (0.67±0.06) and are smaller than those of VPm neurons. We tested how well our model predicts the differences between L4 RSU OFF and ON responses by driving the model with two firing rates whose amplitude ratio is 0.8, approximating the OFF/ON ratio of VPm neurons both in sham and in CA rats (Shoykhet et al., 2012). No other changes were made to model parameters. The resulting OFF/ON ratio is 0.65 in the sham model and 0.69 in the CA model. These simulated OFF/ON ratios fall within the standard errors of experimentally observed values, suggesting that our model, developed initially to account for PW and AW responses, similarly approximates ON and OFF responses in sham and in CA animals.

Correlation of neural activity in sham and CA rats

Correlation of neural activity likely plays an important role in functionally connecting different brain regions (Fries, 2005) as well as in efficiently activating postsynaptic targets by synchronous presynaptic neural populations (Bruno and Sakmann, 2006). However, excessive neural correlation can be detrimental for stimulus coding and discrimination (Averbeck et al., 2006), and active mechanisms normally maintain relatively low stimulus-induced correlations among cortical cells (Ecker et al., 2010; Renart et al., 2010; Ly et al., 2012; Middleton et al., 2012). To examine correlations in sensory stimulation-evoked

662 neuronal activity, we plotted joint PSTHs (jPSTHs; see Methods) of
663 simultaneously recorded responses of L4 RSUs to PW deflections. The peak of
664 the raw jPSTH for jointly recorded CA neurons is smaller than the peak of the
665 jPSTH for sham neurons (Fig. 7A), consistent with smaller PW-evoked
666 responses in CA vs sham rats (Fig. 3). The shuffle-corrected jPSTH, which more
667 closely reflects within-network rather than externally driven stimulus-dependent
668 correlations, reveals higher levels of above chance coincidence in CA neurons
669 compared to sham (Fig. 7B). Since coincidence of two Poisson processes
670 increases as their frequency increases even if the two processes are entirely
671 independent, we further normalized the diagonal of the shuffle-corrected jPSTH
672 by the product of individual PSTHs to get true correlation. The normalized,
673 shuffle-corrected jPSTH in Figure 7C still shows increased correlation among L4
674 RSUs in CA compared to sham rats. Such increases are likely to lead to poorer
675 discrimination among stimuli in CA animals (see Discussion).

676 In order to better understand the potential mechanism of increased
677 correlation in PW-evoked spiking among CA RSUs, we simulated joint activity of
678 pairs of neurons. We made a fraction of excitatory and inhibitory synaptic inputs
679 common to both model neurons using a correlation coefficient, c (see Methods).
680 We set c = 0.15, a value consistent with low correlation among L4 RSUs
681 observed experimentally (Khatri et al., 2009). All other parameters in the model
682 remained unchanged. Raw, shuffle-corrected and normalized jPSTHs for model
683 neurons (Fig. 8) are in good agreement with experimental data (Fig. 7). Thus,

684 high correlation in synaptic inputs leads to greater correlations in firing among CA
685 RSUs vs. sham RSUs.
686
687 **Discussion**
688 In this study, we examined how cardiac arrest during development
689 impacts the function of cortical circuits in adulthood. We found that months after
690 initial injury, responses to principal whisker deflections are smaller in magnitude
691 in CA animals compared to sham rats, while responses to adjacent whisker
692 deflections are comparable in the two groups. A disproportionate decrease in
693 PW-evoked responses leads to broadening of receptive fields among L4 barrel
694 RSU's. Mathematical modeling suggests that increased background
695 conductance of individual neurons, without any other alterations in cellular
696 function or synaptic circuitry, can account for the observed broadening of
697 receptive fields. We also found that spiking activity of barrel neurons is more
698 correlated in CA animals compared to sham rats, indicating more synchronous
699 firing in CA survivors. Together, *in vivo* and modeling data suggest that CA and
700 resuscitation during development permanently affect cortical circuit function in
701 survivors.
702
703 *Cortical circuit function after a hypoxic-ischemic insult*
704 Receptive field broadening effected by decreased magnitude of most robust
705 responses may be a general feature of cortical circuit dysfunction after hypoxic-
706 ischemic injury. In an experimental model of neonatal hypoxia-ischemia in 3 day

707 old mice, epicranial mapping during recovery revealed depressed sensory
708 responses in the primary somatosensory cortex (Quairiaux et al., 2010). Similarly
709 in the mouse visual system, responses in the primary visual cortex are reduced
710 in survivors of neonatal hypoxia-ischemia (Failor et al., 2010). And neurons in
711 the primary auditory cortex display reduced response amplitudes and broadened
712 tuning curves in rats subjected to two 12 minute-long periods of asphyxia shortly
713 after birth (Strata et al., 2010). These studies, encompassing multiple sensory
714 modalities, and our current results show that hypoxic-ischemic insults result in
715 less responsive and more broadly tuned cortical circuits.
716
717 *Potential mechanisms of cortical circuit dysfunction after CA*
718 Our mathematical modeling indicates that an increase in background synaptic
719 conductance of barrel RSU's can account both for smaller PW-evoked responses
720 and for larger AW/PW ratios in RSU's of CA survivors. Prior combined
721 experimental/modeling studies demonstrate how changes in background
722 synaptic conductance modulate response gain (Chance et al., 2002). Balanced
723 increases in background excitatory and inhibitory conductances increase
724 membrane voltage variability, decrease input resistance and shorten membrane
725 time constants, effectively shunting external synaptic inputs (Bernander et al.,
726 1991). Together, these effects shunt synaptic inputs, reducing the slope of input-
727 output firing curve and decreasing the gain. The decrease in gain, in turn,
728 disproportionately reduces responses to stronger stimuli, e.g. PW-evoked
729 deflections. Hence, cortical neurons in a 'high conductance state' integrate

730 spatiotemporal information differently than neurons with less active background
731 synaptic activity (Destexhe et al., 2003).

732 Animal models of global ischemia have uncovered a number of anatomical
733 and synaptic changes during post-injury periods. Among these changes are a
734 transient change in spine density and persistent changes in the distribution of
735 dendritic branching points (Ruan et al., 2007) and the relative prevalence of
736 different spine morphologies (Ruan et al., 2009). To show that different gain
737 control mechanisms can lead to the same results that we observe
738 experimentally, we simulated an injury model where the increased net excitation
739 and inhibition were implemented as an increase in the peak conductance of
740 individual synaptic events. The overall rate of presynaptic input remained the
741 same. By increasing the maximal conductance we observe a decreased gain, but
742 overall higher firing rate of the CA model output (Fig. 9, black dashed line). With
743 an additional decrease in the bias current driving the model (13% decrease) we
744 are able to get a quantitative agreement of the FI-curve to that of the original CA
745 model (Fig. 9, gray dashed line). These findings highlight that there are
746 potentially different physiologic mechanisms of implementing gain control by
747 altering background inhibition and excitation in a concerted manner. However,
748 these results, together with the results of Figure 6, support the hypothesis that
749 alterations in both excitatory and inhibitory circuitry in the cortex underlie reduced
750 PW-driven responses and less well-defined whisker receptive fields in CA
751 survivors.

752 Decreased effective inhibition alone cannot account for our results. For
753 example, sensory deprivation during development, followed by a period of
754 whisker re-growth, leads to increased AW/PW ratios of L4 RSU's via doubling of
755 connection probability between VPm neurons and RSU's (Simons et al., 2015)
756 and effective net decrease in intrabarrel inhibition (Shoykhet et al., 2005). The
757 effect of sensory deprivation, however, is to increase AW-evoked responses out
758 of proportion to the PW-evoked responses, which leads to increased AW/PW
759 ratios via a mechanism distinctly different from that observed in CA survivors.
760 Consistent with population models (Kyriazi and Simons, 1993; Pinto et al., 2003)
761 and *in vivo* data (Kyriazi et al., 1996), reduced inhibition in our model increased
762 AW-evoked firing rates out of proportion to the PW-evoked rates (data not
763 shown). Thus, reducing intra-cortical inhibition alone increases AW/PW ratios,
764 but it cannot explain decreased PW-evoked and preserved AW-evoked response
765 magnitudes we observed in CA survivors.

766 The finding of increased synchrony among L4 RSUs in CA survivors lends
767 further support to the hypothesis that background synaptic conductances are
768 increased in the barrel circuit after CA. Modeling data indicate that introducing
769 an identical degree of correlation into synaptic inputs results in higher correlation
770 among RSUs in the CA circuit than in the sham circuit. Input synaptic correlation
771 was introduced in the model through background conductance. In the CA model
772 background conductance represents a larger proportion of the entire membrane
773 conductance. As a result, the relative input correlation is higher in the CA model
774 than in the sham model. Higher relative input correlation is transferred to the

output function, resulting in higher spiking correlation in the CA model. The ability of the model to reproduce experimentally-determined firing statistics of simultaneously recorded L4 RSUs in CA and sham rats suggests that a balanced increase in background excitatory and inhibitory conductances may indeed be the mechanism underlying functional changes in the barrel circuit of cardiac arrest survivors. This hypothesis can be tested experimentally using *in vivo* intracellular recordings (Wilent and Contreras, 2005).

Behavioral implications of broadened receptive fields and increased spiking coherence

Broadened receptive fields of barrel RSU's in CA survivors will likely degrade the barrel circuit's capacity to differentiate between sensory stimuli arising from individual whiskers. In population coding, well-tuned neurons with small receptive fields generally outperform broadly-tuned neurons with large receptive fields (Zhang and Sejnowski, 1999; Averbeck et al., 2006). Behaviorally, enlarged barrel RSU receptive fields are associated with permanently degraded texture-discrimination capacity in rats deprived of normal sensory input during development (Carvell and Simons, 1996). Although the mechanism of receptive field broadening likely differs between sensory-deprived animals and CA survivors, the detrimental impact on whisker-barrel system function is likely to be similar.

Increased coherence among barrel RSU's may also affect whisker-based behaviors. Coherence among neurons in a given population may increase the

probability of stimulus detection in that population's post-synaptic target (Salinas and Sejnowski, 2001; Middleton et al., 2009). Thus, increased coherence among barrel RSU's may be a beneficial adaptation that compensates for reduced firing rates in CA survivors and improves stimulus detection. The price for this benefit, however, may be reduced stimulus discrimination (Wang et al., 2010). Modeling studies suggest that the detrimental impact of increased coherence on neuronal population coding increases with the size of the population – specifically increased coherence leads to a decrease in stimulus discriminability from population responses (Averbeck et al., 2006). Each Layer IV barrel contains 4000-5000 neurons (Meyer et al., 2010). In a neuronal population of this size, increased coherence can lead to a substantial decrease in discriminability among sensory input signals (Averbeck et al., 2006). Thus, increased coherence among barrel RSU's in CA survivors may further decrease the stimulus coding capacity of the barrel circuit. Whisker-based object detection and texture discrimination may thus represent sensitive behavioral tests of putative therapeutic strategies in cardiac arrest survivors.

Bibliography and References Cited

AHA (2006) 2005 American Heart Association (AHA) guidelines for cardiopulmonary resuscitation (CPR) and emergency cardiovascular care (ECC) of pediatric and neonatal patients: pediatric advanced life support. Pediatrics 117:e1005-1028.

Akhtar ND, Land PW (1991) Activity-dependent regulation of glutamic acid decarboxylase in the rat barrel cortex: effects of neonatal versus adult sensory deprivation. J Comp Neurol 307:200-213.

Atkins DL, Everson-Stewart S, Sears GK, Daya M, Osmond MH, Warden CR, Berg RA (2009) Epidemiology and outcomes from out-of-hospital cardiac arrest in children: the Resuscitation Outcomes Consortium Epistry-Cardiac Arrest. Circulation 119:1484-1491.

Aufderheide TP, Frascone RJ, Wayne MA, Mahoney BD, Swor RA, Domeier RM, Olinger ML, Holcomb RG, Tupper DE, Yannopoulos D, Lurie KG (2011) Standard cardiopulmonary resuscitation versus active compression-decompression cardiopulmonary resuscitation with augmentation of negative intrathoracic pressure for out-of-hospital cardiac arrest: a randomised trial. Lancet 377:301-311.

Averbeck BB, Latham PE, Pouget A (2006) Neural correlations, population coding and computation. Nat Rev Neurosci 7:358-366.

Beaulieu C (1993) Numerical data on neocortical neurons in adult rat, with special reference to the GABA population. Brain Res 609:284-292.

Bernander O, Douglas RJ, Martin KA, Koch C (1991) Synaptic background activity influences spatiotemporal integration in single pyramidal cells. Proc Natl Acad Sci U S A 88:11569-11573.

Bernard SA, Gray TW, Buist MD, Jones BM, Silvester W, Gutteridge G, Smith K (2002) Treatment of comatose survivors of out-of-hospital cardiac arrest with induced hypothermia. N Engl J Med 346:557-563.

Bernard SA, Smith K, Cameron P, Masci K, Taylor DM, Cooper DJ, Kelly AM, Silvester W (2010) Induction of therapeutic hypothermia by paramedics after resuscitation from out-of-hospital ventricular fibrillation cardiac arrest: a randomized controlled trial. Circulation 122:737-742.

Bickler PE, Warren DE, Clark JP, Gabatto P, Gregersen M, Brosnan H (2012) Anesthetic protection of neurons injured by hypothermia and rewarming: roles of intracellular Ca2+ and excitotoxicity. Anesthesiology 117:280-292.

Bottiger BW, Schmitz B, Wiessner C, Vogel P, Hossmann KA (1998) Neuronal stress response and neuronal cell damage after cardiocirculatory arrest in rats. J Cereb Blood Flow Metab 18:1077-1087.

Bruno RM, Simons DJ (2002) Feedforward mechanisms of excitatory and inhibitory cortical receptive fields. J Neurosci 22:10966-10975.

Bruno RM, Sakmann B (2006) Cortex is driven by weak but synchronously active thalamocortical synapses. Science 312:1622-1627.

Carvell GE, Simons DJ (1996) Abnormal tactile experience early in life disrupts active touch. J Neurosci 16:2750-2757.

CDC (2002) State-specific mortality from sudden cardiac death--United States, 1999. MMWR Morb Mortal Wkly Rep 51:123-126.

Chance FS, Abbott LF, Reyes AD (2002) Gain modulation from background synaptic input. Neuron 35:773-782.

De Maio VJ, Stiell IG, Wells GA, Spaite DW (2003) Optimal defibrillation response intervals for maximum out-of-hospital cardiac arrest survival rates. Ann Emerg Med 42:242-250.

Deasy C, Bernard SA, Cameron P, Jaison A, Smith K, Harriss L, Walker T, Masci K, Tibballs J (2010) Epidemiology of paediatric out-of-hospital cardiac arrest in Melbourne, Australia. Resuscitation 81:1095-1100.

Dembrow NC, Chitwood RA, Johnston D (2010) Projection-specific neuromodulation of medial prefrontal cortex neurons. J Neurosci 30:16922-16937.

Destexhe A, Rudolph M, Pare D (2003) The high-conductance state of neocortical neurons in vivo. Nat Rev Neurosci 4:739-751.

Ecker AS, Berens P, Keliris GA, Bethge M, Logothetis NK, Tolias AS (2010) Decorrelated neuronal firing in cortical microcircuits. Science 327:584-587.

Failor S, Nguyen V, Darcy DP, Cang J, Wendland MF, Stryker MP, McQuillen PS (2010) Neonatal cerebral hypoxia-ischemia impairs plasticity in rat visual cortex. J Neurosci 30:81-92.

Fink EL, Alexander H, Marco CD, Dixon CE, Kochanek PM, Jenkins LW, Lai Y, Donovan HA, Hickey RW, Clark RS (2004) Experimental model of pediatric asphyxial cardiopulmonary arrest in rats. Pediatr Crit Care Med 5:139-144.

Fries P (2005) A mechanism for cognitive dynamics: neuronal communication through neuronal coherence. Trends Cogn Sci 9:474-480.

Gabbiani, Cox (2010) Mathematics for Neuroscientists, 1st Edition. London, UK: Academic Press.

Geocadin RG, Muthuswamy J, Sherman DL, Thakor NV, Hanley DF (2000) Early electrophysiological and histologic changes after global cerebral ischemia in rats. Mov Disord 15 Suppl 1:14-21.

Gottschalk A, Burmeister MA, Freitag M, Cavus E, Standl T (2002) Influence of early defibrillation on the survival rate and quality of life after CPR in prehospital emergency medical service in a German metropolitan area. Resuscitation 53:15-20.

Graves JR, Herlitz J, Bang A, Axelsson A, Ekstrom L, Holmberg M, Lindqvist J, Sunnerhagen K, Holmberg S (1997) Survivors of out of hospital cardiac arrest: their prognosis, longevity and functional status. Resuscitation 35:117-121.

Higley MJ, Contreras D (2006) Balanced excitation and inhibition determine spike timing during frequency adaptation. J Neurosci 26:448-457.

Hossmann KA, Oschlies U, Schwindt W, Krep H (2001) Electron microscopic investigation of rat brain after brief cardiac arrest. Acta Neuropathol 101:101-113.

Inan M, Crair MC (2007) Development of cortical maps: perspectives from the barrel cortex. Neuroscientist 13:49-61.

912 Johnston MV, Hagberg H (2007) Sex and the pathogenesis of cerebral palsy.
913 Dev Med Child Neurol 49:74-78.
914 Karch SB, Graff J, Young S, Ho CH (1998) Response times and outcomes for
915 cardiac arrests in Las Vegas casinos. Am J Emerg Med 16:249-253.
916 Khatri V, Hartings JA, Simons DJ (2004) Adaptation in thalamic barreloid and
917 cortical barrel neurons to periodic whisker deflections varying in frequency
918 and velocity. J Neurophysiol 92:3244-3254.
919 Khatri V, Bruno RM, Simons DJ (2009) Stimulus-specific and stimulus-
920 nonspecific firing synchrony and its modulation by sensory adaptation in
921 the whisker-to-barrel pathway. J Neurophysiol 101:2328-2338.
922 Kumar K, White BC, Krause GS, Indrieri RJ, Evans AT, Hoehner TJ, Garritano
923 AM, Koestner A (1988) A quantitative morphological assessment of the
924 effect of lidoflazine and deferoxamine therapy on global brain ischaemia.
925 Neurol Res 10:136-140.
926 Kyriazi HT, Simons DJ (1993) Thalamocortical response transformations in
927 simulated whisker barrels. J Neurosci 13:1601-1615.
928 Kyriazi HT, Carvell GE, Brumberg JC, Simons DJ (1996) Quantitative effects of
929 GABA and bicuculline methiodide on receptive field properties of neurons
930 in real and simulated whisker barrels. J Neurophysiol 75:547-560.
931 Land PW, Simons DJ (1985) Cytochrome oxidase staining in the rat SmI barrel
932 cortex. J Comp Neurol 238:225-235.
933 Land PW, de Blas AL, Reddy N (1995) Immunocytochemical localization of
934 GABAA receptors in rat somatosensory cortex and effects of tactile
935 deprivation. Somatosens Mot Res 12:127-141.
936 Lefort S, Tomm C, Floyd Sarria JC, Petersen CC (2009) The excitatory neuronal
937 network of the C2 barrel column in mouse primary somatosensory cortex.
938 Neuron 61:301-316.
939 Lisman JE, Fellous JM, Wang XJ (1998) A role for NMDA-receptor channels in
940 working memory. Nat Neurosci 1:273-275.
941 Ly C, Middleton JW, Doiron B (2012) Cellular and circuit mechanisms maintain
942 low spike co-variability and enhance population coding in somatosensory
943 cortex. Front Comput Neurosci 6:7.
944 Mateen FJ, Josephs KA, Trenerry MR, Felmlee-Devine MD, Weaver AL, Carone
945 M, White RD (2011) Long-term cognitive outcomes following out-of-
946 hospital cardiac arrest: A population-based study. Neurology.
947 Matos RI, Watson RS, Nadkarni VM, Huang HH, Berg RA, Meaney PA, Carroll
948 CL, Berens RJ, Praestgaard A, Weissfeld L, Spinella PC (2013) Duration
949 of cardiopulmonary resuscitation and illness category impact survival and
950 neurologic outcomes for in-hospital pediatric cardiac arrests. Circulation
951 127:442-451.
952 Meyer HS, Wimmer VC, Oberlaender M, de Kock CP, Sakmann B, Helmstaedter
953 M (2010) Number and laminar distribution of neurons in a thalamocortical
954 projection column of rat vibrissal cortex. Cereb Cortex 20:2277-2286.
955 Middleton JW, Longtin A, Benda J, Maler L (2009) Postsynaptic receptive field
956 size and spike threshold determine encoding of high-frequency

information via sensitivity to synchronous presynaptic activity. J Neurophysiol 101:1160-1170.

Middleton JW, Omar C, Doiron B, Simons DJ (2012) Neural correlation is stimulus modulated by feedforward inhibitory circuitry. J Neurosci 32:506-518.

Mitchell SJ, Silver RA (2003) Shunting inhibition modulates neuronal gain during synaptic excitation. Neuron 38:433-445.

Moler FW et al. (2015) Therapeutic hypothermia after out-of-hospital cardiac arrest in children. N Engl J Med 372:1898-1908.

Myers RE, Yamaguchi S (1977) Nervous system effects of cardiac arrest in monkeys. Preservation of vision. Arch Neurol 34:65-74.

Oswald AM, Reyes AD (2008) Maturation of intrinsic and synaptic properties of layer 2/3 pyramidal neurons in mouse auditory cortex. J Neurophysiol 99:2998-3008.

Oswald AM, Reyes AD (2011) Development of inhibitory timescales in auditory cortex. Cereb Cortex 21:1351-1361.

Paxinos G, Watson C (2007) The rat brain in stereotaxic coordinates, 6th Edition. Amsterdam ; Boston ;: Academic Press/Elsevier.

Pidoux M, Mahon S, Deniau JM, Charpier S (2011) Integration and propagation of somatosensory responses in the corticostriatal pathway: an intracellular study in vivo. J Physiol 589:263-281.

Pinto DJ, Hartings JA, Brumberg JC, Simons DJ (2003) Cortical damping: analysis of thalamocortical response transformations in rodent barrel cortex. Cereb Cortex 13:33-44.

Pulsinelli WA, Brierley JB (1979) A new model of bilateral hemispheric ischemia in the unanesthetized rat. Stroke 10:267-272.

Quairiaux C, Sizonenko SV, Megevand P, Michel CM, Kiss JZ (2010) Functional deficit and recovery of developing sensorimotor networks following neonatal hypoxic-ischemic injury in the rat. Cereb Cortex 20:2080-2091.

Radovsky A, Katz L, Ebmeyer U, Safar P (1997) Ischemic neurons in rat brains after 6, 8, or 10 minutes of transient hypoxic ischemia. Toxicol Pathol 25:500-505.

Radovsky A, Safar P, Sterz F, Leonov Y, Reich H, Kuboyama K (1995) Regional prevalence and distribution of ischemic neurons in dog brains 96 hours after cardiac arrest of 0 to 20 minutes. Stroke 26:2127-2133; discussion 2133-2124.

Renart A, de la Rocha J, Bartho P, Hollender L, Parga N, Reyes A, Harris KD (2010) The asynchronous state in cortical circuits. Science 327:587-590.

Roger VL et al. (2012) Heart disease and stroke statistics--2012 update: a report from the American Heart Association. Circulation 125:e2-e220.

Ruan YW, Lei Z, Fan Y, Zou B, Xu ZC (2009) Diversity and fluctuation of spine morphology in CA1 pyramidal neurons after transient global ischemia. J Neurosci Res 87:61-68.

Ruan YW, Zou B, Fan Y, Li Y, Lin N, Zhang Y, Xu ZC (2007) Morphological heterogeneity of CA1 pyramidal neurons in response to ischemia. J Neurosci Res 85:193-204.

1003 Salinas E, Sejnowski TJ (2001) Correlated neuronal activity and the flow of
1004 neural information. Nat Rev Neurosci 2:539-550.
1005 Schreckinger M, Geocadin RG, Savonenko A, Yamashita S, Melnikova T, Thakor
1006 NV, Hanley DF (2007) Long-lasting cognitive injury in rats with apparent
1007 full gross neurological recovery after short-term cardiac arrest.
1008 Resuscitation 75:105-113.
1009 Shoykhet M, Simons DJ (2008) Development of thalamocortical response
1010 transformations in the rat whisker-barrel system. J Neurophysiol 99:356-
1011 366.
1012 Shoykhet M, Land PW, Simons DJ (2005) Whisker trimming begun at birth or on
1013 postnatal day 12 affects excitatory and inhibitory receptive fields of layer
1014 IV barrel neurons. J Neurophysiol 94:3987-3995.
1015 Shoykhet M, Simons DJ, Alexander H, Hosler C, Kochanek PM, Clark RS (2012)
1016 Thalamocortical dysfunction and thalamic injury after asphyxial cardiac
1017 arrest in developing rats. J Neurosci 32:4972-4981.
1018 Simons DJ (1978) Response properties of vibrissa units in rat SI somatosensory
1019 neocortex. J Neurophysiol 41:798-820.
1020 Simons DJ (1983) Multi-whisker stimulation and its effects on vibrissa units in rat
1021 SmI barrel cortex. Brain Res 276:178-182.
1022 Simons DJ, Carvell GE (1989) Thalamocortical response transformation in the rat
1023 vibrissa/barrel system. J Neurophysiol 61:311-330.
1024 Simons DJ, Carvell GE, Kyriazi HT (2015) Alterations in functional
1025 thalamocortical connectivity following neonatal whisker trimming with adult
1026 regrowth. J Neurophysiol 114:1912-1922.
1027 Softky WR, Koch C (1993) The highly irregular firing of cortical cells is
1028 inconsistent with temporal integration of random EPSPs. J Neurosci
1029 13:334-350.
1030 Statler KD, Alexander H, Vagni V, Holubkov R, Dixon CE, Clark RS, Jenkins L,
1031 Kochanek PM (2006) Isoflurane exerts neuroprotective actions at or near
1032 the time of severe traumatic brain injury. Brain Res 1076:216-224.
1033 Strata F, Stoianov IP, de Villers-Sidani E, Bonham B, Martone T, Kenet T, Chang
1034 EF, Vincenti V, Merzenich MM (2010) Perinatal asphyxia affects rat
1035 auditory processing: implications for auditory perceptual impairments in
1036 neurodevelopmental disorders. PLoS One 5:e15326.
1037 The Hypothermia after Cardiac Arrest Study Group H (2002) Mild therapeutic
1038 hypothermia to improve the neurologic outcome after cardiac arrest. N
1039 Engl J Med 346:549-556.
1040 Valenzuela TD, Roe DJ, Cretin S, Spaite DW, Larsen MP (1997) Estimating
1041 effectiveness of cardiac arrest interventions: a logistic regression survival
1042 model. Circulation 96:3308-3313.
1043 Van der Loos H, Woolsey TA (1973) Somatosensory cortex: structural alterations
1044 following early injury to sense organs. Science 179:395-398.
1045 Wang HE, Devlin SM, Sears GK, Vaillancourt C, Morrison LJ, Weisfeldt M,
1046 Callaway CW (2012) Regional variations in early and late survival after
1047 out-of-hospital cardiac arrest. Resuscitation 83:1343-1348.

1048 Wang Q, Webber RM, Stanley GB (2010) Thalamic synchrony and the adaptive
1049 gating of information flow to cortex. Nat Neurosci 13:1534-1541.
1050 Weigl M, Tenze G, Steinlechner B, Skhirtladze K, Reining G, Bernardo M,
1051 Pedicelli E, Dworschak M (2005) A systematic review of currently
1052 available pharmacological neuroprotective agents as a sole intervention
1053 before anticipated or induced cardiac arrest. Resuscitation 65:21-39.
1054 Weisfeldt ML, Everson-Stewart S, Sitlani C, Rea T, Aufderheide TP, Atkins DL,
1055 Bigham B, Brooks SC, Foerster C, Gray R, Ornato JP, Powell J,
1056 Kudenchuk PJ, Morrison LJ (2011) Ventricular tachyarrhythmias after
1057 cardiac arrest in public versus at home. N Engl J Med 364:313-321.
1058 Wilent WB, Contreras D (2005) Dynamics of excitation and inhibition underlying
1059 stimulus selectivity in rat somatosensory cortex. Nat Neurosci 8:1364-
1060 1370.
1061 Wong-Riley MT, Merzenich MM, Leake PA (1978) Changes in endogenous
1062 enzymatic reactivity to DAB induced by neuronal inactivity. Brain Res
1063 141:185-192.
1064 Zhang K, Sejnowski TJ (1999) Neuronal tuning: To sharpen or broaden? Neural
1065 Comput 11:75-84.
1066 Zive D, Koprowicz K, Schmidt T, Stiell I, Sears G, Van Ottingham L, Idris A,
1067 Stephens S, Daya M (2011) Variation in out-of-hospital cardiac arrest
1068 resuscitation and transport practices in the Resuscitation Outcomes
1069 Consortium: ROC Epistry-Cardiac Arrest. Resuscitation 82:277-284.
1070

Figure Legends

Figure 1. *Response of layer 4 single RS units in whisker/barrel cortex of sham and CA rats*. **A** The rat whisker pad consists of an ordered array of order whiskers; as an example, filled black circles indicate whisker D3 as the PW, and whiskers D2 and D4 as AWs in the same row and whiskers C3 and E3 as AWs in the same column. **B** To characterize spatial receptive field properties (relative responses across the whisker array) we recorded from neurons while stimulating their primary whisker (PW; see Materials and Methods) and 2-4 adjacent whiskers (AWs), individually, in either the same column or same row as the PW. **C** An example tangential section of the L4 barrel field stained for cytochrome oxidase (see Methods) illustrating an electrolytic lesion to confirm the location of the primary whisker. **D** In response to a 1mm "ramp-and-hold" whisker deflection (see Materials and Methods) an L4 RSU responds with a robust, transient increase in firing rate. After the whisker deflection offset, the unit responds with a similar, albeit smaller, transient increase in firing rate. The shaded area schematically represents the time window for computing the ON response. **E** A representative waveform of a single-unit RS neuron recording. All recorded waveforms are shown in gray. The average waveform is shown in black. **F** The ISI histogram for all recorded units in Sham rats. The ISI histogram in CA rats is essentially identical (not shown). Bin width 1 ms. **G** The first 5 ms of the ISI histogram in panel F. Note absence of recorded spikes in the absolute refractory period of 1 ms. **H** The set of spike time responses of an example sham neuron, presented a spike time raster plot, illustrates the sparseness of spontaneous activity and relative robustness of whisker evoked responses. **I** The peristimulus time histogram (PSTH) of a representative RSU from a sham rat in response to PW deflection (asterisks indicate onset and offset times) indicates a robust, temporally precise response (top). The responses to the 4 AWs are smaller in amplitude, and in at least one case (AW_2) there is no appreciable response. **J** An L4 RSU from a CA rat displays a small PW-evoked response similar in magnitude to those evoked by some of the AWs (AW_1 and AW_2).

Figure 2. *Receptive field properties of regular spike neurons in layer 4*. **A** Adjacent whisker (AW) to principle whisker (PW) response ratios are larger in CA neurons (0.49 ± 0.03; n=57), than in sham neurons (0.23 ± 0.03; n=34; WRST, p=0.0002). **B** Mean spike counts (observed in a 25 ms window after whisker deflection), in response to PW deflections, are larger for sham neurons (0.89 ± 0.11) than for CA neurons (0.50 ± 0.04; WRST, p=0.0002). **C** Sham and CA neurons have similar AW-evoked spike count responses (sham: 0.18 ± 0.03; CA: 0.21 ± 0.02; WRST, p=0.6846).

Figure 3. *Barrel and cortical laminar cytoarchitecture in sham and CA rats*. **A** Cytochrome oxidase (CO) histology reveals a well-ordered somatotopic map of the whisker array in layer 4 primary somatosensory cortex in sham rats. **B** No apparent gross abnormalities were observed in the barrel cytoarchitecture in CA animals. **C-D**. Normal gross brain morphology in CA rats (**D**) compared to sham

rats (**C**). Nissl stain. Scale bar 1 mm. **E-F**. Preserved cortical laminar structure in CA rats (**F**) compared to sham rats (**E**). Images enlarged from panels **D** and **C**, respectively. Scale bar 0.5 mm. Notice neuronal loss in the CA1 region of the hippocampus.

Figure 4. *Subthreshold membrane and spiking properties of sham and CA model neurons*. **A** When spiking threshold is removed, the mean voltage of the sham model (gray) increases with increases in input firing rate. The mean voltage for the CA model (black) starts at higher levels, but increases more slowly with increasing input rate. The reduced gain of membrane voltage arises from a higher level of balanced background excitatory and inhibitory fluctuating conductances. The higher conductance shunts a higher proportion of the feedforward inputs. **B** Consistent with increased shunting observed for the mean depolarization, the integration of single synaptic inputs is smaller for the CA model (black) than for the sham model (gray). **C** Both sham (left) and CA (right) models fire at comparable rates when driven with input rates corresponding to spontaneous levels (top row). Similarly, input firing rates corresponding to AW-evoked thalamic inputs result in comparable output rates in both models (middle row). However, high level of input firing, corresponding to PW-evoked thalamic inputs (bottom row), effectively drives the sham model (left), but fails to drive the CA model to high levels (right).

Figure 5. *Input output relations and AW/PW responses of layer 4 sham and CA model neurons*. Static firing rate-input (FI) curves for the sham model (gray) and CA model (black) neurons are calculated as a function of the firing rate of the feedforward input pathway. The lower traces show the range of instantaneous firing rates spanned by the simulated PW (solid line) and AW (dashed line) feedforward inputs in the dynamic models. At the level of spontaneous input firing rates, the output FI curves have similar values for both sham and CA models. For peak AW input firing rates the FI curves for sham and CA models also have similar stationary output firing rates; the sham AW response is slightly higher than the CA AW response. In contrast, the FI curve for the sham model is much higher at the level of peak PW input rates than the FI curve for the CA model.

Figure 6. *Peristimulus time histograms (PSTHs) of real and model neurons in response to PW and AW whisker deflections.* **A** The average PSTH of layer 4 neurons from sham rats in response to a whisker deflection beginning at 0 ms. The PW PSTH rapidly increases to high instantaneous firing rates and then relaxes more slowly to spontaneous rates (solid gray), while the AW PSTH peaks at smaller values (dashed gray). In contrast, the average PW PSTH peaks at a smaller rate (solid black), relative to sham neurons, while the AW PSTH (dashed black) peaks at similar values to the sham neurons. PSTHs are calculated using 1 ms bins. Instantaneous firing rates are calculated by dividing the observed counts by 1 ms. **B** Sham and CA model neurons reproduce the relative PW and AW PSTH responses. The sham PW PSTH (solid gray) peaks at a higher

instantaneous firing rate relative to the CA model (solid black), while the sham (dashed gray) and CA (dashed black) AW PSTHs peak at similar values.

Figure 7. *Pairwise correlation structure in sham and CA layer 4 RSUs*. **A** The average joint peristimulus time histogram (jPSTH) of pairs of layer 4 excitatory neurons reveals a robust co-activation in response to whisker deflection in sham neurons (left). CA neuron coincident firing is smaller as revealed by a lower magnitude jPSTH (right). Comparing the projections of the jPSTHs along the diagonal gives the temporal profile of the cross-correlation at lag zero. **B** Shuffle-corrected jPSTHs (see Materials and Methods) reveal higher levels of coincident firing in CA vs sham RSUs. **C** Normalizing the cross-correlation from the shuffle-corrected jPSTHs by the peak value of the raw jPSTHs (see Materials and Methods) reveals a larger relative correlation for L4 RSU in CA rats.

Figure 8. *Pairwise correlation structure in sham and CA model layer 4 RSUs*. **A** The average jPSTH of pairs of layer 4 model neurons reveals a robust co-activation in response to whisker deflection in sham neurons (left). CA neuron coincident firing is smaller in magnitude as revealed by a lower magnitude jPSTH (right). Comparing the projections of the jPSTHs along the diagonal gives the temporal profile of the cross-correlation at lag zero. **B** Subtracting the shuffle-corrected jPSTHs (see Materials and Methods) reveals more similar sham and CA jPSTH structure. **C** The normalized cross-correlation reveals a larger relative correlation for CA model neurons that is qualitatively consistent with the experimental data in Fig. 7.

Figure 9. *Alternate mechanisms of gain control in CA model neurons*. The original sham and CA model from Fig. 5 are shown in solid gray and black curves. The dashed black line shows increased gain of the FI curve when the maximum amplitude of a unitary background input, instead of the net background conductance event rate as in the original CA model, is increased. The overall firing rate, however, is also increased, which is inconsistent with experimental data. Decreasing the mean bias current slightly shifts the FI curve (gray dashes) downward to match the data and the original CA model.

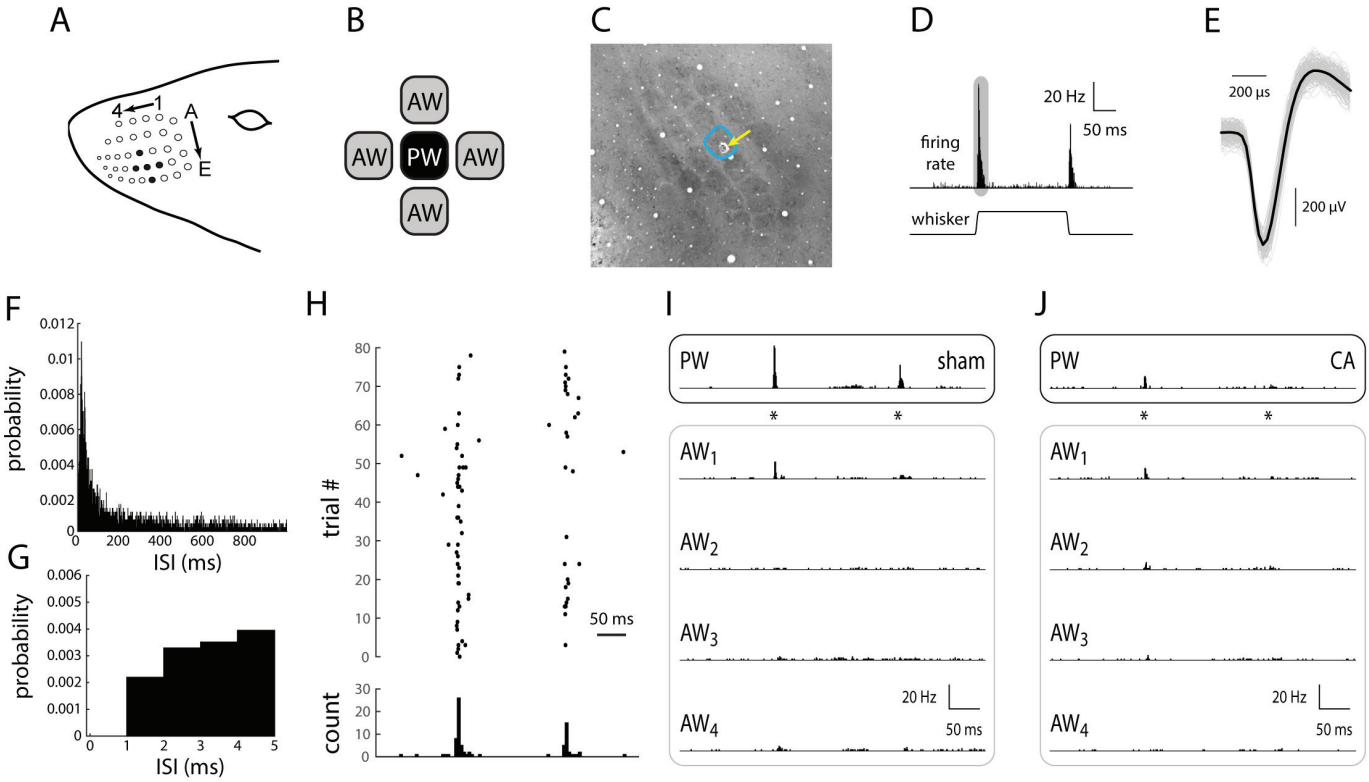

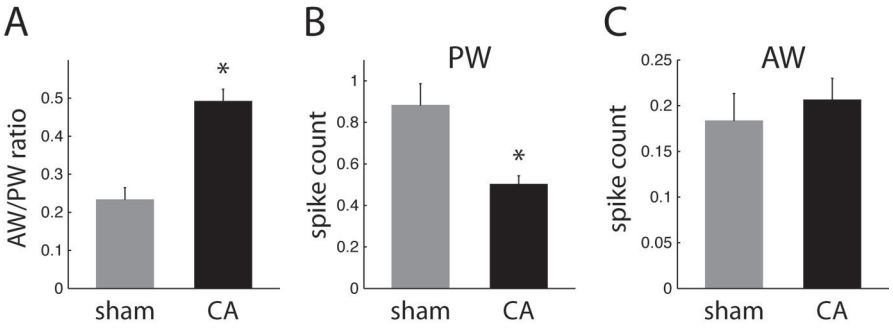

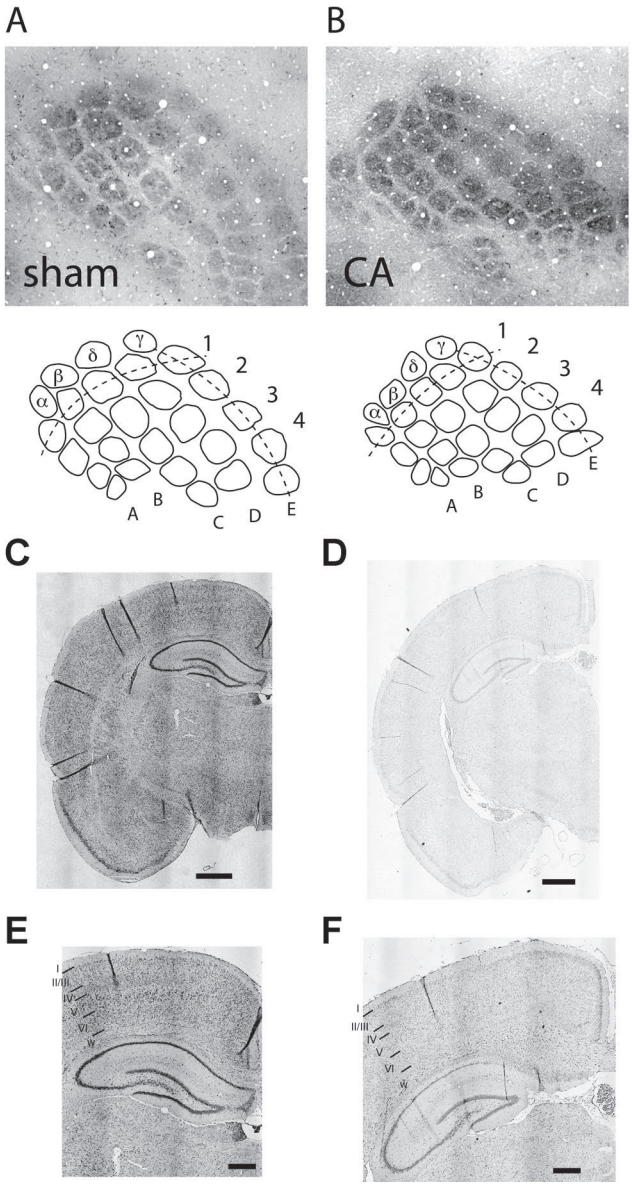

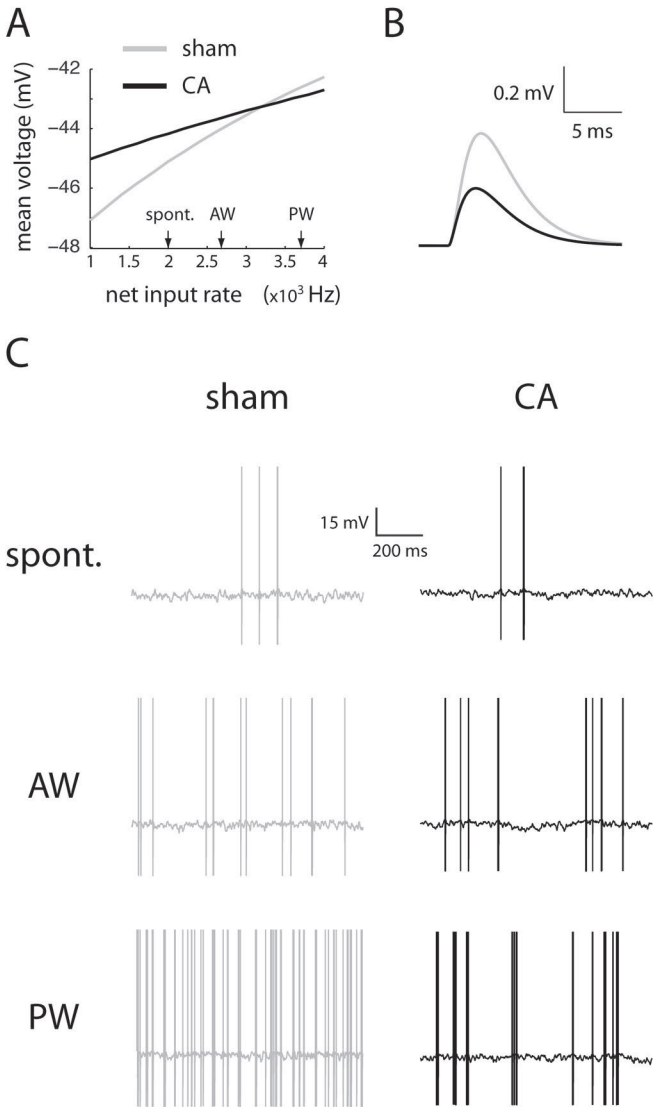

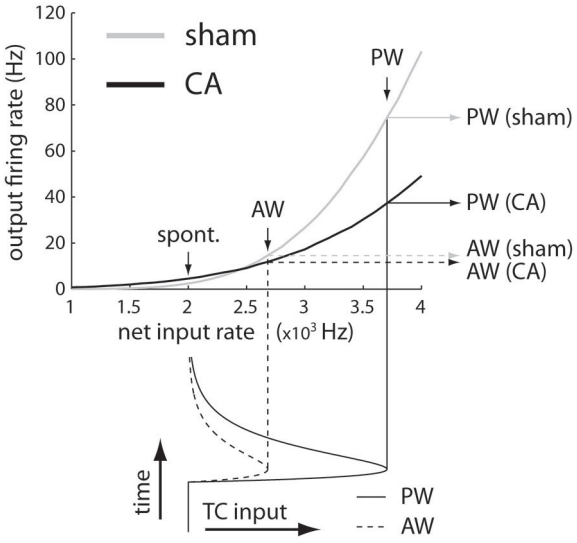

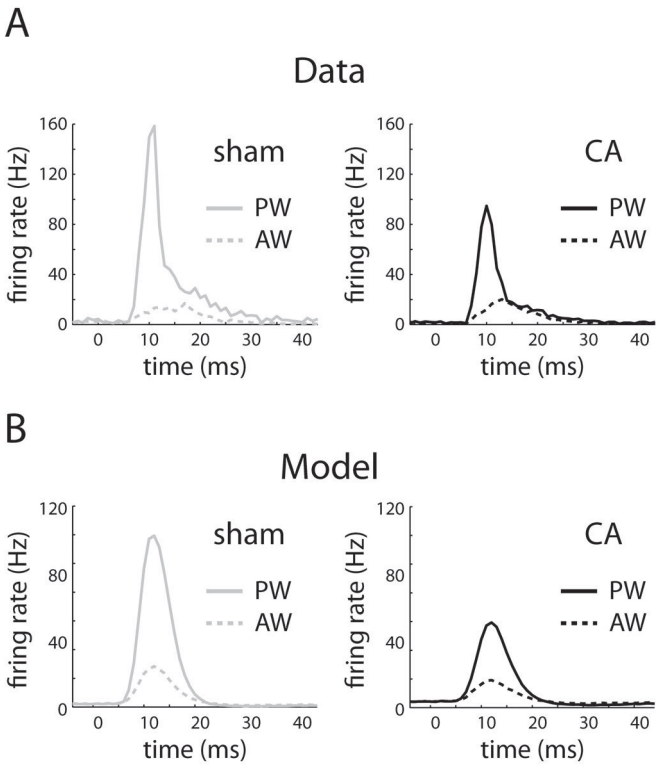

A

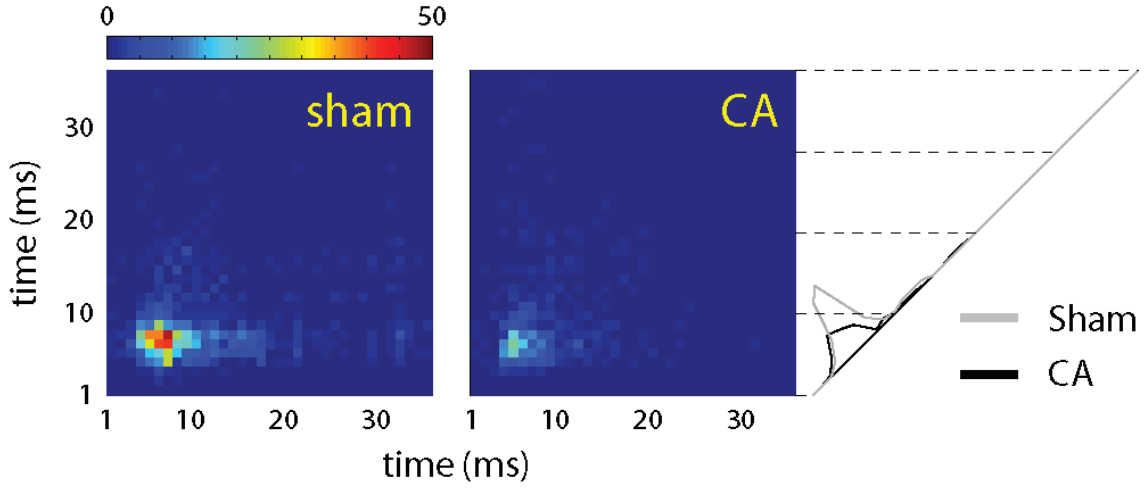

B

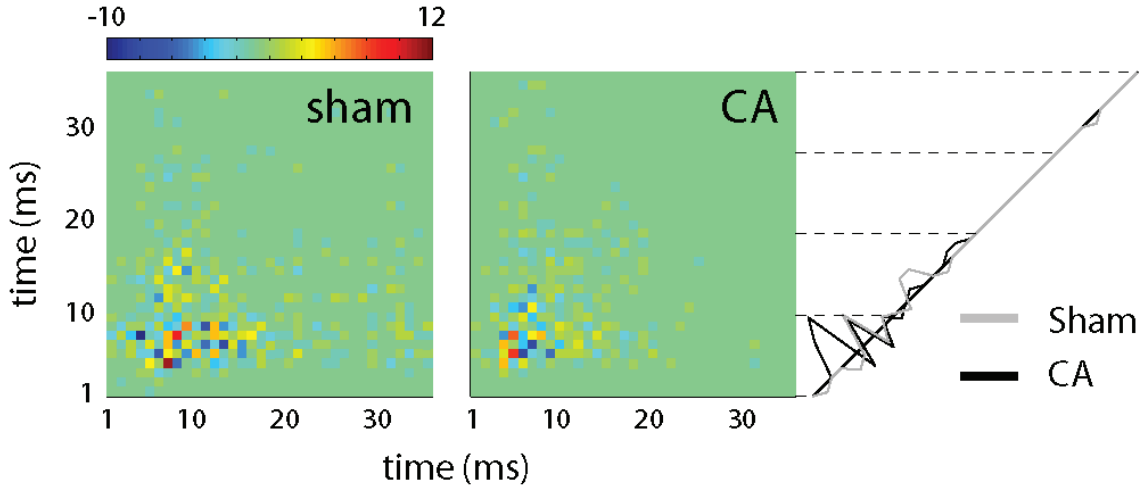

C

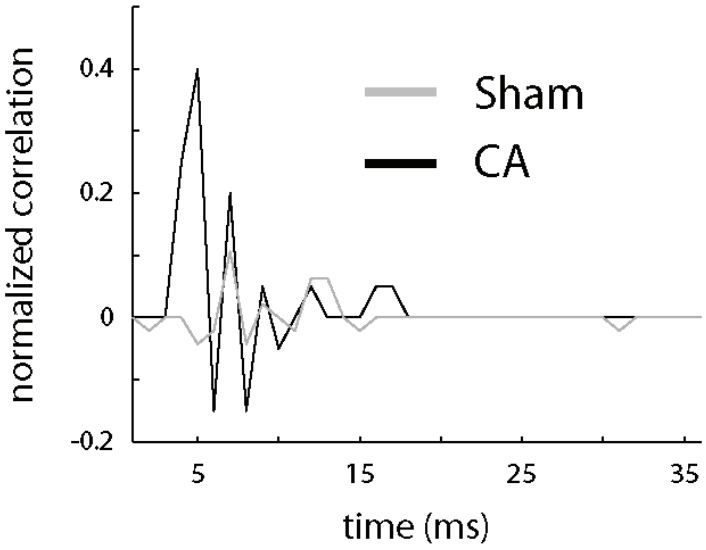

A

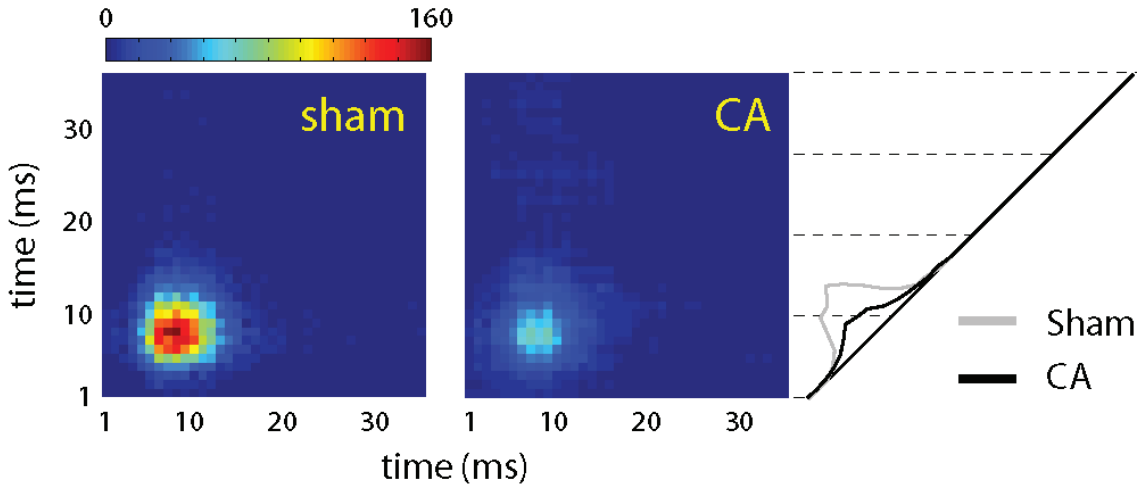

B

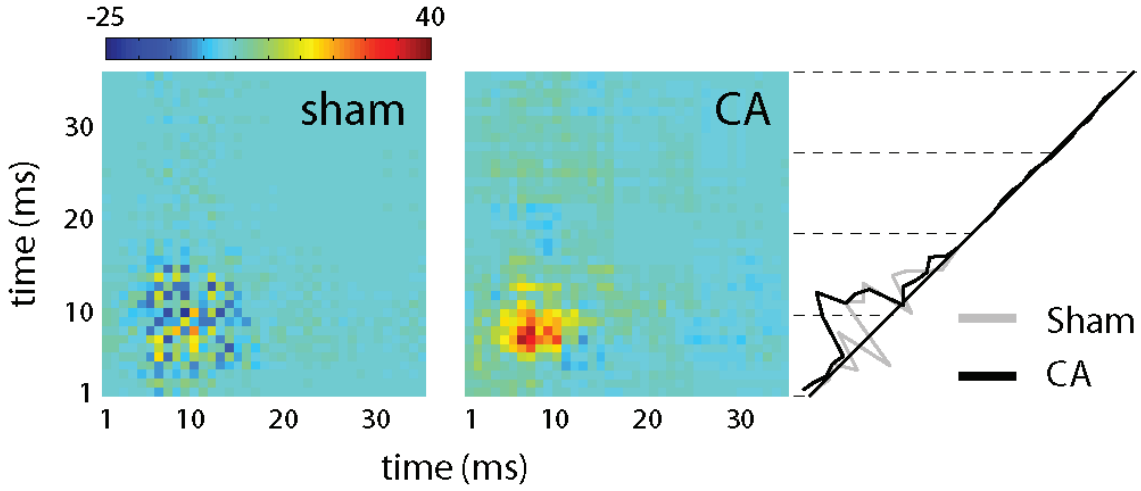

C